AJNR

Detection of Intracranial Hemorrhage with Susceptibility-Weighted MR Sequences

Luxia Liang, Yukunori Korogi, Takeshi Sugahara, Yoshinori Shigematsu, Tomoko Okuda, Ichiro Ikushima and Mutsumasa Takahashi

AJNR Am J Neuroradiol 1999, 20 (8) 1527-1534
http://www.ajnr.org/content/20/8/1527

AJNR Am J Neuroradiol 20:1527–1534, September 1999

Detection of Intracranial Hemorrhage with Susceptibility-Weighted MR Sequences

Luxia Liang, Yukunori Korogi, Takeshi Sugahara, Yoshinori Shigematsu, Tomoko Okuda, Ichiro Ikushima, and Mutsumasa Takahashi

BACKGROUND AND PURPOSE: **Detection of hemorrhage is important in the diagnosis and management of a variety of intracranial diseases. We evaluated the sensitivity of the following sequences for depicting chronic hemorrhagic foci associated with susceptibility dephasing: gradient-recalled echo (GRE) imaging, GRE-type single-shot echo-planar imaging (GRE-EPI), spin-echo–type single-shot echo-planar imaging (SE-EPI), turbo spin-echo (TSE) imaging, half-Fourier single-shot turbo spin-echo (HASTE) imaging, and segmented HASTE (s-HASTE) imaging. To our knowledge, no previous comparison has been made with these techniques in the same patient.**

METHODS: **Fifty patients with suspected chronic hemorrhage were examined prospectively with the above six sequences. Contrast-to-noise ratio (CNR), sensitivity to detection of lesions, conspicuity of internal architecture, and sensitivity to small hemorrhagic foci were evaluated.**

RESULTS: **Hemorrhagic foci were found in 35 patients. The CNR of the GRE, GRE-EPI, SE-EPI, TSE, s-HASTE, and HASTE sequences was 30.9, 23.7, 3.6, 6.1, −29.3, and −13.1, respectively; the number of small hemorrhagic foci detected was 85, 96, 44, 22, two, and one, respectively, for the supratentorial white matter; 70, 40, 19, four, zero, and zero, respectively, for the supratentorial cortical/subcortical region; and 73, 50, 26, 37, zero, and zero, respectively, for the infratentorial/skull-base region.**

CONCLUSION: **The GRE sequence was best for detecting susceptibility dephasing associated with chronic intracranial hemorrhage. GRE-EPI, while comparable to GRE in the supratentorial compartment, was reduced in its sensitivity near the skull base, and may be used as an alternative to GRE in uncooperative, unsedated, pediatric, or claustrophobic patients. SE-EPI should not be used in screening for intracranial hemorrhage.**

The detection of hemorrhage is important in the diagnosis and management of a variety of intracranial diseases, including hypertensive hemorrhage, hemorrhagic infarction, brain tumor, cerebral aneurysm, vascular malformation, trauma, hemorrhagic change following radio- or chemotherapy, and hemorrhagic pial metastasis (1–4). A recent report has indicated that the detection of hemorrhage on MR images is useful for the grading of gliomas (2). The T2-weighted gradient-recalled echo (GRE) sequence has been reported to be more sensitive than the T2-weighted spin-echo (SE) and fast SE sequences to the magnetic susceptibility induced by static field inhomogeneities arising from paramagnetic blood breakdown products (1, 5–11).

Recently, ultrafast sequences have been developed and applied clinically because of their remarkable time savings and minimization of motion artifacts, especially in uncooperative, medically unstable, or claustrophobic patients (12–15). These sequences may be classified into two groups according to data acquisition techniques. One uses a fast SE technique and includes half-Fourier acquisition single-shot turbo spin-echo (HASTE) and segmented-HASTE (s-HASTE) sequences, which are acquired with multiple 180° refocusing pulses. Another uses the GRE technique and includes GRE-type echo-planar imaging (GRE-EPI) and SE-type echo-planar imaging (SE-EPI), which are acquired with the use of multiple gradient reversals. Both the GRE-EPI and SE-EPI techniques are sensitive to susceptibility effects and are thus generally used for perfusion-sensitive MR imaging and functional MR imaging (16–18). One group of investigators reported that the GRE-EPI sequence might be more sensitive to hyperacute hemorrhage than the GRE technique (5). The HASTE sequences have proved less sensitive to hemorrhagic suscep-

Received September 8, 1998; accepted after revision May 10, 1999.

From the Department of Radiology, Kumamoto University School of Medicine, 1-1-1 Honjo, Kumamoto 860-8556, Japan.

Address reprint requests to Yukunori Korogi, MD.

TABLE 1: Parameters used for six imaging sequences

	GRE	GRE-EPI	SE-EPI	TSE	s-HASTE	HASTE
TR/TE/excitations	500/15/2	1000/46/1	1000/97/1	3700/96/1	8000/82/1	2040/95/1
Flip angle	15°	· · ·	· · ·	· · ·	· · ·	· · ·
Matrix	192 × 256	148 × 256	126 × 256	224 × 256	128 × 256	240 × 256
FOV (mm)	265 × 199	265 × 265	265 × 265	200 × 175	265 × 265	265 × 265
Section thickness (mm)	5	5	5	5	5	5
Gap (mm)	1	1	1	1	1	1
Echo train length	· · ·	· · ·	· · ·	7	64	128
Bandwidth (Hz/pixel)	78	833	833	65	260	260
Acquisition time*	3 min, 27 s	3–4 s	3–4 s	2 min, 7 s	16 s	30–38 s

Note.—GRE indicates gradient-echo sequence; GRE-EPI, GRE–type echo-planar imaging; SE-EPI, spin-echo–type echo-planar imaging; TSE, turbo spin-echo sequence; HASTE, half-Fourier acquisition single-shot turbo spin-echo sequence; s-HASTE, segmented-HASTE sequence.

* Acquisition time is for the entire sequence (15–20 sections).

tibility in preliminary studies (1, 12, 19). Nevertheless, no previous comparison has been made with these sequences in the same patients.

Our study was undertaken to compare differences in the detection of susceptibility dephasing caused by various chronic hemorrhages among six T2- or T2*-weighted MR imaging sequences: the turbo spin-echo (TSE), s-HASTE, and HASTE sequences, and the susceptibility-weighted sequences, including GRE fast low-angle shot (FLASH), GRE-EPI, and SE-EPI. We also sought to determine whether the EPI sequences can be used as an alternative to the GRE sequence for detection of chronic hemorrhage.

Methods

Patients

Prospective comparison of the GRE, GRE-EPI, SE-EPI, TSE, s-HASTE, and HASTE sequences was performed in 50 consecutive patients in whom intracranial hemorrhage was suspected. Twenty-seven patients were male and 23 were female; ages ranged from 17 to 71 years (mean, 43 years). Hemorrhagic complications were from brain tumor (n = 30), arteriovenous malformation (AVM) (n = 6), cavernous angioma (n = 5), chronic hemorrhagic infarction (n = 3), chronic hematoma (n = 2), hemorrhage of brain tumor following biopsy (n = 2), neurosyphilis (n = 1), and brain contusion (n = 1). No patient with relatively acute hemorrhage was included in the study. All the brain tumors, the one cavernous angioma, and the one case of neurosyphilis were proved by histologic specimens obtained from surgery or biopsy. All AVMs were confirmed by digital subtraction angiography. The other diagnoses were based on a combination of clinical information and MR or CT findings. Plain CT scans (with 7-mm-thick sections) were obtained in all patients within 15 days before the MR examination (38 cases) or within 1 week after the MR examination (12 cases).

MR Imaging

MR imaging was performed on a 1.5-T unit. After conventional T1-weighted imaging (600–700/14–24 [TR/TE]), the above six sequences were obtained in the axial plane with a section thickness of 5 mm and an intersection gap of 1 mm. The same scout and orientation were used for all sequences. The imaging parameters of the six sequences are shown in Table 1. Contrast-enhanced T1-weighted and contrast-enhanced magnetization-prepared rapid acquisition gradient-echo (MP-RAGE) sequences were also obtained in the axial plane in all patients with brain tumors and in some of the other patients. Parameters for the MP-RAGE sequence were 13.5/7; inversion time/delay time, 300/300; flip angle, 15°; section thickness, 1.5 mm; slab thickness, 13.5 cm; matrix: 224 × 256; acquisition time, 6 minutes. MR angiography was performed in all patients with an AVM or hematoma.

Image Interpretation

Paramagnetic blood products associated with chronic hemorrhagic foci were assumed present if hypointense foci were recognized on T2- or T2*-weighted MR images. Signal voids of vascular structures were confirmed by combined appraisal of T1-weighted, contrast-enhanced T1-weighted, and MR angiographic sequences. Final interpretation was reached by consensus of the two neuroradiologists. Hypointensity due to calcification was excluded by comparison with the corresponding level on CT scans. Bilateral symmetric hypointensity of the basal ganglia due to physiologic deposition of calcification or iron was also excluded in our study. Because inherent signal characteristics and unique artifacts always differentiated the six sequences, the sequences could not be graded in a blinded fashion.

Quantitative Analysis.—Signal intensity was measured in the hypointense lesions with a circular region of interest (ROI) on each sequence by one of the researchers. The lesions equal to or greater than 10 mm in diameter on the GRE sequence were chosen for the contrast-to-noise ratio (CNR) measurement in order to minimize the partial volume effects. If the patient had more than three lesions, three lesions were randomly selected for the measurement of signal intensity. If the lesion was not well depicted on a sequence, we put the ROI at the corresponding area. Signal intensity in the white matter was obtained in areas of the centrum semiovale excluding pathologic lesions. Signal intensity of the normal white matter and background noise were measured with matching ROIs. The CNRs for lesions and white matter were derived in all six sequences by using the following formula: $CNR = (SI_{WM} - SI_L)/SD$, where SI_L is the mean signal intensity of the ROI within the lesion; SI_{WM}, the mean signal intensity of the white matter; and SD, the standard deviation of noise along the phase-encoding direction. Individual sequences were compared by using a paired *t*-test. Difference were considered statistically significant if the *P* value was less than .01.

Qualitative Analysis.—Two experienced neuroradiologists reviewed all images for lesions greater than or equal to 5 mm in diameter on the GRE sequence to determine whether these lesions could be detected on all other sequences. The two observers scored them on a four-point scale as follows: grade 0 (negative), no hypointensity visible; grade 1 (poor), hypointensity vaguely visible; grade 2 (fair), hypointensity visible but with poor delineation; and grade 3 (good), hypointensity clearly visible with good delineation. Since susceptibility effects of

hemorrhage could also interfere with visualization of the internal signal intensity of a lesion, such as a tumor or cavernous angioma, conspicuity of the internal architecture and of the margin of the lesion were also evaluated as we scored the detection of the hemorrhagic foci. These were scored on a four-point scale as follows: grade 0 (negative), no internal structure or margin visible; grade 1 (poor), internal structure and margin vaguely visible; grade 2 (fair), internal structure visible but margin blurred; and grade 3 (good), both the internal structure and the margin clearly visible. In addition, the reader was also asked to comment on the corresponding lesion size on all six sequences. Statistical analysis was performed by using one-factor analysis of variance (ANOVA) to determine statistically significant differences between two groups. Differences were considered statistically significant if the *P* value was less than .05.

Finally, the sensitivities of the sequences for detection of small lesions (<5.0 mm) were evaluated. Initially, two neuroradiologists independently counted the number of the lesions on each sequence. The final decision was made by means of consensus of the two radiologists as to whether a lesion seen on an image obtained with one sequence could be seen on an image obtained with a different sequence in a side-by-side analysis. The locations of the lesions were divided into supratentorial white matter, supratentorial cortical-subcortical area, infratentorial and skull-base area, and postcraniotomy site.

Results

Thirty-six patients had an area of hypointensity on at least one of the six T2- and T2*-weighted sequences. One ganglioglioma proved to have giant calcification without hemorrhage by plain CT. Four brain tumors with hypointense lesions proved to have hemorrhage as well as discrete calcification within them. Existence of calcification was excluded in all other hypointense lesions by plain CT. As a result, 35 patients (18 men, 17 women; age range, 19 to 67 years; mean age, 46 years) with chronic hemorrhagic foci were studied for comparison. Disorders among these patients included brain tumor (n = 20), cavernous angioma (n = 5), AVM (n = 3), chronic hemorrhagic infarction (n = 3), chronic hematoma (n = 2), and hemorrhage of brain tumor following biopsy (n = 2).

Quantitative Analysis

The CNRs were measured in 27 lesions of 16 patients on the six sequences. The CNRs for the GRE, GRE-EPI, SE-EPI, TSE, S-HASTE, and HASTE sequences were 30.9 ± 11.9, 23.7 ± 9.0, 3.6 ± 6.6, 6.1 ± 14.1, −29.3 ± 30.1, and −13.1 ± 15.0, respectively. The GRE and GRE-EPI sequences had higher CNRs than any of the other sequences ($P < .0001$). The CNR of the GRE sequence was significantly higher than that of the GRE-EPI sequence ($P = .0008$). The TSE and SE-EPI sequences had higher CNRs than the s-HASTE and HASTE sequences ($P < .0001$). There was no significant difference in CNR between the TSE and SE-EPI sequences ($P = .83$) or between the s-HASTE and HASTE sequences ($P = .02$), although the CNR of the TSE sequence was slightly better than that of the SE-EPI sequence (Figs 1A and 2).

Qualitative Analysis

Thirty-six hemorrhagic lesions in 25 patients were assessed for their detectability and for the conspicuity of their internal architecture. For detection of the lesions, the GRE and GRE-EPI sequences had the highest scores ($P < .0001$). The TSE and SE-EPI sequences were superior to the s-HASTE and HASTE sequences ($P < .0001$). There was no significant difference between the GRE and GRE-EPI sequences ($P = .73$), between the TSE and SE-EPI sequences ($P = .42$), or between the s-HASTE and HASTE sequences ($P = .44$) (Figs 1B and 2). For conspicuity of the internal architecture, the GRE and TSE sequences had the highest score and were significantly superior to the other sequences. The SE-EPI and GRE-EPI sequences had the lowest scores. No significant difference was found between the GRE and TSE sequences ($P = .70$), between the HASTE and s-HASTE sequences ($P = .39$), between the SE-EPI and GRE-EPI sequences ($P = .81$), between the s-HASTE and SE-EPI sequences ($P = .13$), or between the s-HASTE and GRE-EPI sequences ($P = .08$) (Fig 1C).

To assess the sensitivity of each sequence, a total of 252 hypointense lesions less than 5 mm in diameter were counted in 18 patients (Table 2). The GRE and GRE-EPI sequences detected more lesions than the TSE and SE-EPI sequences. No lesions were detected by the SE-EPI and TSE sequences that were not depicted by the GRE or GRE-EPI sequences. Among the six sequences, the s-HASTE and HASTE sequences were the least sensitive in the detection of small lesions. The GRE-EPI sequence was relatively superior to the GRE sequence in the detection of lesions in the supratentorial white matter but inferior in the detection of lesions in other areas (Fig 3). In the supratentorial white matter, 14 lesions were detected by the GRE-EPI sequence, while only three lesions were detected by the GRE sequence alone. However, 32 lesions in the supratentorial cortical/subcortical areas and 27 lesions in the infratentorial/skull-base areas were detected by the GRE sequence alone, while two lesions in the supratentorial cortical/subcortical areas and four lesions in the infratentorial/skull-base areas were detected by the GRE-EPI sequence alone. The SE-EPI sequence delineated more supratentorial lesions but fewer infratentorial lesions than the TSE sequence. Compared with the GRE sequence, the size of the susceptibility effect associated with the hemorrhagic foci was larger with the GRE-EPI and SE-EPI sequences and smaller with the TSE sequence (Figs 2 and 3).

Discussion

Our findings regarding sensitivity for detecting susceptibility dephasing associated with chronic hemorrhage among the six imaging sequences may be summarized as follows: the GRE and GRE-EPI sequences were the most sensitive, followed by the

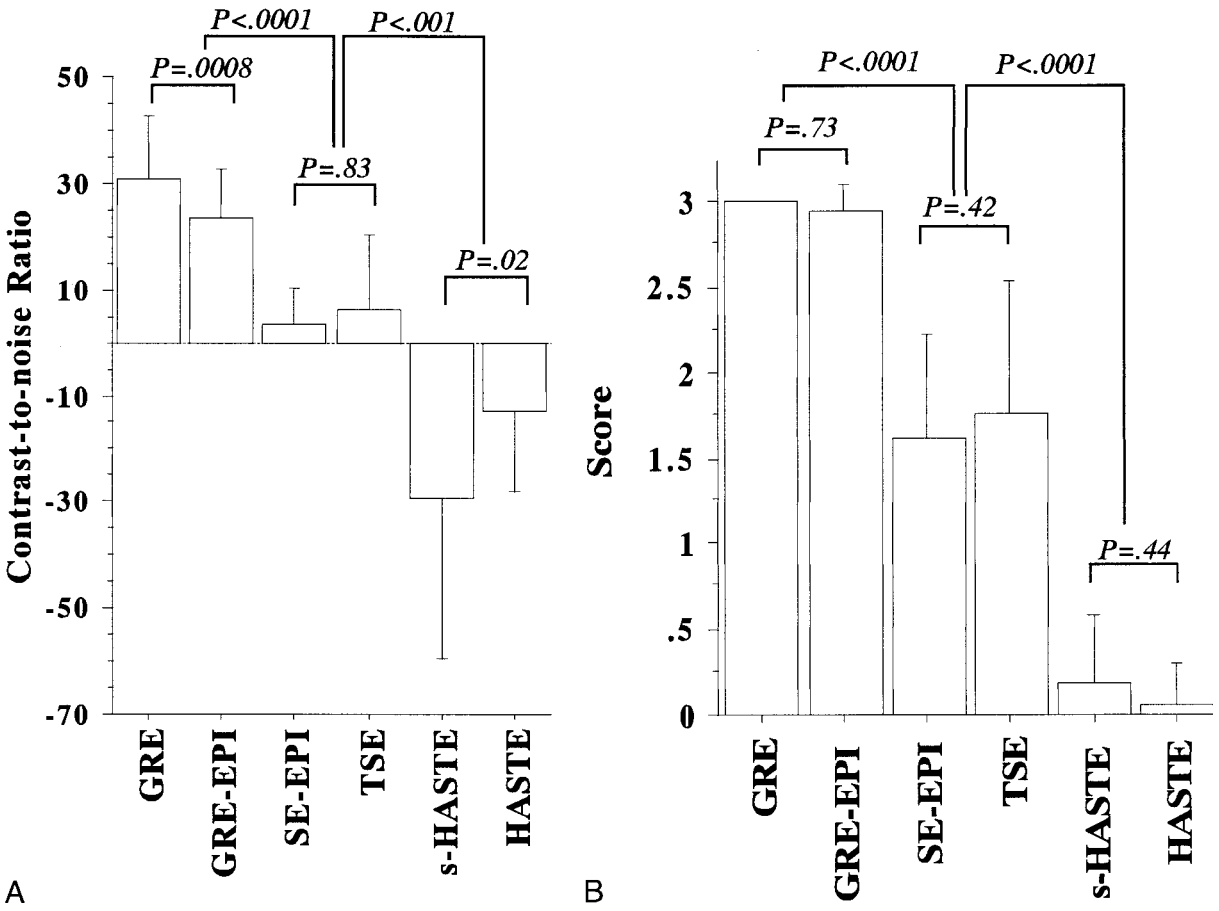

FIG 1. *A–C,* Quantitative and qualitative analysis among the six sequences for CNR (*A*), lesion detection (*B*), and conspicuity of internal architecture (*C*). GRE indicates gradient-echo sequence; GRE-EPI, GRE-type echo-planar imaging; SE-EPI, spin-echo–type echo-planar imaging; TSE, turbo spin-echo sequence; HASTE, half-Fourier acquisition single-shot turbo spin-echo sequence; s-HASTE, segmented-HASTE sequence.

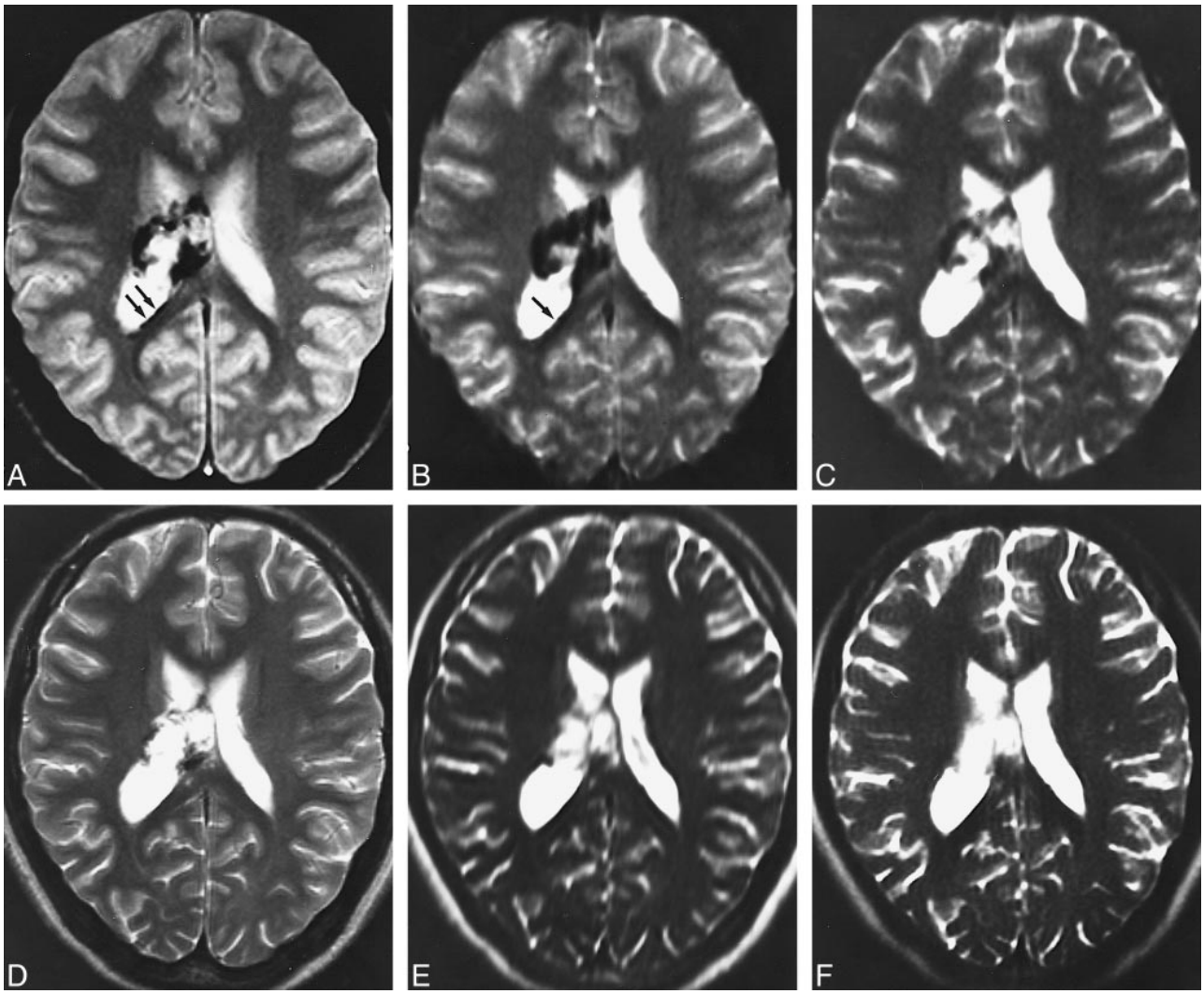

FIG 2. Intraventricular anaplastic astrocytoma in a 19-year-old woman.

A and *B,* The GRE (*A*) and GRE-EPI (*B*) images clearly show the intratumoral hemorrhage; however, the size of the hypointense area is larger on the GRE-EPI image than on the GRE image. The linear hemorrhage along the right ventricular wall (*arrows*) is seen on the GRE image only.

C and *D,* Contrast between the hemorrhage and the white matter is poorer on the SE-EPI (*C*) and TSE (*D*) images than on the GRE and GRE-EPI images.

E and *F,* Hemorrhage is poorly seen on the s-HASTE (*E*) and HASTE (*F*) images.

TABLE 2: Number of small lesions (<5 mm) detected by the six sequences

Site	Total	GRE	GRE-EPI	SE-EPI	TSE	s-HASTE	HASTE	Only by GRE	Only by GRE-EPI
Supratentorial									
White matter	99	85	96	44	22	2	1	3	14
Cortex/subcortex	72	70	40	19	4	0	0	32	2
Infratentorial/skull base	77	73	50	26	37	0	0	27	4
Postcraniotomy site	4	4	1	0	1	0	0	3	0

Note.—GRE indicates gradient-echo sequence; GRE-EPI, GRE–type echo-planar imaging; SE-EPI, spin-echo–type echo-planar imaging; TSE, turbo spin-echo sequence; HASTE, half-Fourier acquisition single-shot turbo spin-echo sequence; s-HASTE, segmented-HASTE sequence.

SE-EPI and TSE sequences; the s-HASTE and HASTE sequences were the least sensitive. The differences among the sequences in the detection of hemorrhagic foci are closely associated with the ability of each sequence to detect susceptibility changes.

Low signal intensity occurs on GRE and GRE-EPI sequences when the spins dephase with T2*

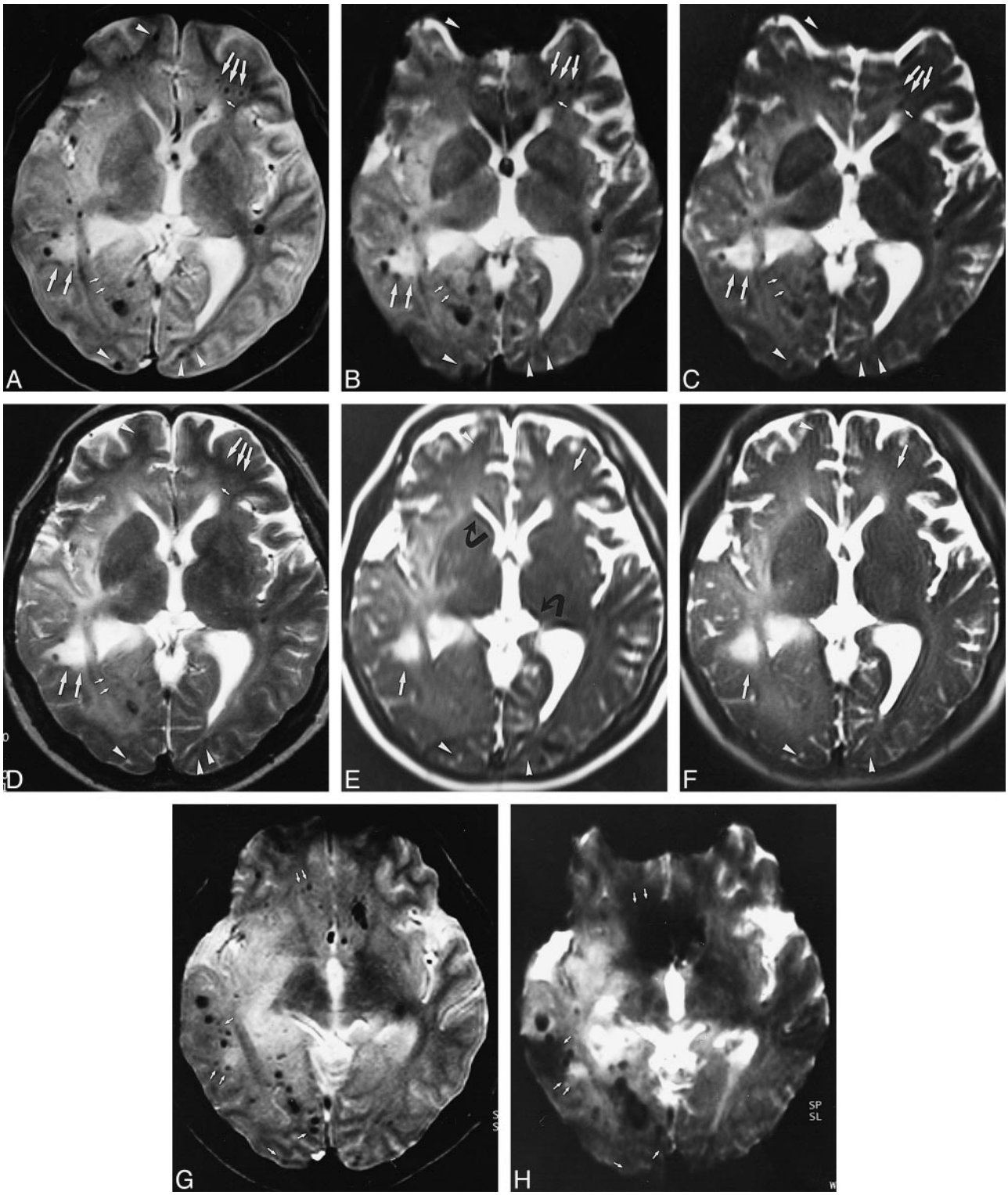

FIG 3. Anaplastic astrocytoma after surgery and radio/chemotherapy in a 32-year-old woman.

A and *B,* Multiple small hemorrhagic lesions (*large arrows*) are detected on the GRE (*A*) and GRE-EPI (*B*) images.The GRE image is more sensitive to the cortical and subcortical lesions (*arrowheads*) than the GRE-EPI image, which is distorted by artifacts from frontal sinuses and calvaria. The GRE-EPI image is more sensitive to the white matter lesions than is the GRE image (*small arrows*).

C and *D,* Fewer lesions are seen on the SE-EPI (*C*) and TSE (*D*) images than on the GRE and GRE-EPI images (*arrows* and *arrowheads*).

E and *F,* The s-HASTE (*E*) and HASTE (*F*) images do not show the small hemorrhagic lesions (*arrows* and *arrowheads*). Note the interface low intensity between CSF and cerebral parenchyma on the s-HASTE image, which should not be mistaken for hemosiderosis (*curved arrow*).

G and *H,* Lower sections around the skull base. Susceptibility artifacts (*arrows*) from the skull base obscure the lesions at the infratentorial and skull-base level on the GRE-EPI image (*H*) and less so on the GRE image (*G*).

relaxation time in the absence of a 180° radiofrequency (RF) refocusing pulse. Inhomogeneity of the primary static magnetic field (B_0) and magnetic susceptibility differences between adjacent tissues are typical sources of such spin dephasing. Signals of the TSE, s-HASTE, and HASTE sequences are acquired during the spin dephase with T2 relaxation time. Their sensitivity to the magnetic susceptibility effect is decreased by the use of multiple refocusing pulses, which rephase both susceptibility-induced dephasing and phase incoherence from inhomogeneities in the applied static magnetic field (6, 20, 21). The 180° RF refocusing pulse compensates for the T2* decay (22, 23); thus, the susceptibility effects of hemorrhage decrease as the number of 180° RF pulses increases (6, 19, 23). No 180° RF refocusing pulse is used in the GRE and GRE-EPI sequences; one is applied in the SE-EPI sequence, seven in the TSE sequence, and numerous in the HASTE and s-HASTE sequences.

The flip angle and TE of the GRE sequence were closely associated with susceptibility effects. A longer TE and larger flip angle may increase the susceptibility effects but degrade the image quality (23). In the study by Atlas et al (6), the longer TE of the GRE sequence probably resulted in its failure to depict 14 of the 61 lesions. It is important to choose an appropriate parameter that balances lesion visibility with image quality.

The small lesions (<5.0 mm in diameter) consisted of post-radio/chemotherapy hemorrhagic foci, occult cavernous angioma, intratumoral microhemorrhage, and hemorrhagic foci in the patient with hypertension. A greater number of small foci within the supratentorial white matter were detected with the GRE-EPI sequence than with the GRE sequence. This difference probably reflects the increased sensitivity to susceptibility artifacts in the GRE-EPI sequence and increased ''blooming'' of lesions with susceptibility changes. The blooming effect was more obvious on the GRE-EPI and SE-EPI sequences than on the GRE and TSE sequences. Because of the blurring of the lesion border on the GRE-EPI sequence, two close lesions usually showed confluent tendencies. Although the blooming effect of the GRE-EPI sequence may decrease the CNR, the enlarged size of susceptibility artifact associated with hemorrhagic foci contributed to the high sensitivity in the clinical cases. Because of its very short scan time and high sensitivity to the supratentorial hemorrhagic foci, the GRE-EPI sequence may be able to substitute for the GRE sequence in the screening of hemorrhage in uncooperative, unsedated, pediatric, or claustrophobic patients.

However, the GRE-EPI sequence was less sensitive than the GRE sequence in the detection of infratentorial/skull-base or postcraniotomy sites because of susceptibility artifacts, poor fat suppression, and image distortion (13). The GRE-EPI sequence was also inferior to the GRE sequence in detecting cortical/subcortical hemorrhagic foci. This may be partly caused by the T2* filtering effects (filtering of high spatial frequencies), which result in blurring of the images due to T2* decay during data collection (13). The T2* decay filtering effects, which may be seen between the gray and white matter or between the gray matter and subarachnoid areas, made actual spatial resolution even worse than expected from the pixel size. Low signal-to-noise ratio and low spatial resolution of the GRE-EPI sequence may also contribute to the poor visualization of the cortical/subcortical lesions (13).

The SE-EPI sequence was significantly inferior to the GRE and GRE-EPI sequences in both quantitative and qualitative evaluations despite the fact that the SE-EPI sequence has been widely used for susceptibility-based functional and perfusion MR imaging. The SE-EPI sequence should not be used in the detection of small hemorrhagic lesions. The signal of the SE-EPI sequence is inherently a gradient-echo technique, but the data acquisition is performed using an oscillation gradient after a single excitation with a 180° refocusing pulse. Our results suggest that this 180° refocusing excitation pulse made the SE-EPI sequence insensitive to many of the small hemorrhagic foci.

The s-HASTE and HASTE sequences were significantly less sensitive than the other sequences in the detection of chronic hemorrhagic foci. These findings are in agreement with previous reports (12, 19). In contrast to the other four sequences, hypointense foci were not seen on the s-HASTE and HASTE sequences. The reasons for insensitivity of the HASTE series are complex. Tissue with a short T2, such as hemorrhage, produces almost no signal in echoes at the end of the pulse train. T2 decay during data collection of s-HASTE and HASTE sequences causes blurring of the images along the phase-encoding direction, because the signal intensity changes substantially over the long readout period (24, 25) and the blurring caused by the T2 decay is very marked for shorter T2 tissue, such as white matter. Therefore, the signal intensity of the white matter becomes quite low, resulting in poor contrast between hemorrhage and white matter (12, 13, 19). The s-HASTE sequence usually showed an artifactual low-signal border at the interface of the CSF and brain parenchyma, which is similar to the findings in superficial siderosis. The cause of this artifact is unknown, but might be related to the fact that tissues with a very long T2 do not fully recover before the second excitation pulse that causes concomitant discontinuities in the k-space trajectories. Care should be taken not to mistake it for hemosiderin deposition.

Depiction of the internal architecture of hemorrhagic lesions is important because the appearance of the internal structure helps us to understand the stage of hematomas or to differentiate idiopathic hemorrhage from hemorrhage caused by pathologic conditions, such as intraaxial tumor or vascular malformation (2, 26). In this regard, the GRE-EPI,

SE-EPI, HASTE, and s-HASTE sequences were not as useful as the GRE and TSE sequences. Although the TSE sequence was the best for visualizing the internal architecture of hemorrhagic foci, the GRE sequence was comparable in quality. Therefore, the GRE sequence may be the optimal choice because of its better sensitivity as well as its comparable visualization of internal architecture.

There are some limitations to this investigation. First, we did not evaluate the conventional SE sequence with dual TEs, although previous investigators found the TSE sequence to be equal to the conventional SE technique for depicting hemorrhage (27). Second, the susceptibility effects evaluated may be caused by many conditions, including flow void, calcification, nonhemorrhagic iron deposition, and other susceptibility artifacts, such as air and hardware associated with the surgical approach. According to Yamada et al (28), calcification other than that which occurs in the basal ganglia may be separated from hemorrhage by a phase image. Although we excluded the possibility of calcification and flow void by use of CT scans, T1-weighted MR images, and MR angiograms, nonhemorrhagic susceptibility artifacts could not be absolutely excluded.

Conclusion

Although scan time is relatively longer, we found the GRE sequence to be the best technique for evaluating foci of chronic intracranial hemorrhage, in part because of its higher sensitivity to susceptibility effects, its better visualization of the internal architecture of hemorrhagic foci, and its reduced distortion at the skull base. The GRE-EPI sequence, which has sensitivity comparable to the GRE sequence in the supratentorial compartment and also a short acquisition time, may be used as an alternative to the GRE sequence for the detection of hemorrhagic foci in uncooperative, unsedated, pediatric, or claustrophobic patients. Limitations of the GRE-EPI sequence include poor visualization of the internal architecture of hemorrhagic foci and decreased sensitivity near the skull base, due to severe image distortion. The SE-EPI, TSE, s-HASTE, and HASTE sequences were inferior to the above two sequences and should not be used to screen for intracranial hemorrhage.

References

1. Bradley WG. **MR appearance of hemorrhage in the brain.** *Radiology* 1993;189:15–26
2. Bagley LJ, Grossman RI, Judy KD, et al. **Gliomas: correlation of magnetic susceptibility artifact with histologic grade.** *Radiology* 1997;202:511–516
3. Spetzler RF, Harggraves RW, McCormick PW, Zabramski JM, Flom RA, Zimmerman RS. **Relationship of perfusion pressure and size to risk of hemorrhage from arteriovenous malformation.** *J Neurosurg* 1992;76:918–923
4. Rabin BM, Meyer JR, Berlin JW, Marymount MH, Palka PS, Russell EJ. **Radiation-induced changes in the central nervous system and head and neck.** *Radiographics* 1996;16:1055–1072
5. Patel MR, Edelman RR, Warach S. **Detection of hyperacute primary intraparenchymal hemorrhage by magnetic resonance imaging.** *Stroke* 1996;27:2321–2324
6. Atlas SW, Mark AS, Grossman RI, et al. **Intracranial hemorrhage: gradient-echo MR imaging at 1.5 T comparison with spin-echo imaging and clinical applications.** *Radiology* 1988; 168:803–807
7. Barr RM, Dillon WP, Wilson CB. **Slow-flow vascular malformations of the pons: capillary telangiectasias?** *AJNR Am J Neuroradiol* 1996;17:71–78
8. Seidenwurm D, Meng TK, Kowalski HK. **Intracranial hemorrhagic lesions: evaluation with spin-echo and gradient-refocused MR imaging at 0.5 and 1.5 T.** *Radiology* 1989;172: 189–194
9. Taber KH, Hayman LA, Herrick RC, et al. **Importance of clot structure in gradient-echo magnetic resonance imaging of hematoma.** *J Magn Reson Imaging* 1996;6:878–883
10. Edelman RR, Johonson K, Buxton R, et al. **MR of hemorrhage: a new approach.** *AJNR Am J Neuroradiol* 1986;7:751–756
11. Pauling L, Coryell CD. **The magnetic properties and structures of hemoglobin, oxyhemoglobinand carbonmonoxyhemoglobin.** *Proc Natl Acad Sci USA* 1936;22:210–216
12. Sugahara T, Korogi Y, Hirai T, et al. **Comparison of HASTE and segmented-HASTE sequences with a T2-weighted fast spin-echo sequence in the screening evaluation of the brain.** *AJR Am J Roentgenol* 1997;169:1401–1410
13. Seiwert B, Patel MR, Mueller MF, et al. **Brain lesions in patients with multiple sclerosis: detection with echo-planar imaging.** *Radiology* 1995;196:765–771
14. Ozdoba C, Remonda L, Heid O, Lovblad KO, Schroth G. **High-resolution echo-planar imaging of the brain: is it suitable for routine clinical imaging.** *Neuroradiology* 1997;39:833–840
15. Simonson TM, Magnotta VA, Ehrhardt JC, Crosby DL, Fisher DJ, Yuh WT. **Echo-planar FLAIR imaging in evaluation of intracranial lesions.** *Radiographics* 1996;16:575–584
16. Edelman RR, Wielopolski PW, Schmitt F. **Echo-planar MR imaging.** *Radiology* 1994;192:600–612
17. Aronen HJ, Gazit IE, Luis DN, et al. **Cerebral blood volume maps of gliomas: comparison with tumor grade and histologic findings.** *Radiology* 1994;191:41–51
18. Sugahara T, Korogi Y, Kochi M, et al. **Correlation of MR imaging–determined cerebral blood volume maps with histologic and angiographic determination of vascularities of gliomas.** *AJR Am J Roentgenol* 1998;171:1479–1486
19. Patel MR, Kulfas RA, Alberico RA, et al. **Half-Fourier acquisition single-shot turbo spin-echo (HASTE) MR: comparison with fast spin-echo MR in diseases of the brain.** *AJNR Am J Neuroradiol* 1997;18:1635–1640
20. Melki PS, Jolesz FA, Mulkern RV. **Partial RF echo-planar imaging with the FAISE method, II: contrast equivalence with spin-echo-sequences.** *Magn Reson Med* 1992;26:342–354
21. Melki PS, Jolesz FA, Mulkern RV. **Partial RF echo-planar imaging with the FAISE method, I: experimental and theoretical assessment of artifacts.** *Magn Reson Med* 1992;26:328–341
22. Pui MH, Fok ECM. **MR imaging of the brain: comparison of gradient-echo and spin-echo pulse sequences.** *AJR Am J Roentgenol* 1995;165:959–962
23. Henkelman M, Kucharczyk W. **Optimization of gradient-echo MR for calcium detection.** *AJNR Am J Neuroradiol* 1994;15: 465–472
24. Melki PS, Mulkenn RV, Panych LP, et al. **Comparing the FAISE method with conventional dural-echo sequences.** *J Magn Reson Imaging* 1991;1:319–326
25. Jara H, Wehrli GW. **Determination of background gradients with diffusion MR imaging.** *J Magn Reson Imaging* 1994;4: 787–797
26. Gomori JM, Grossman RI. **Mechanisms responsible for the MR appearance and evolution of intracranial hemorrhage.** *Radiographics* 1988;8:427–440
27. Jones KM, Mulkern RV, Mantello, MT. **Brain hemorrhage: evaluation with fast spin-echo and conventional dual spin-echo images.** *Radiology* 1992;182:53–58
28. Yamada M, Imakita S, Sakuma T. **Intracranial calcification on gradient-echo phase image: depiction of diamagnetic susceptibility.** *Radiology* 1996;198:171–178